Phenotypic integration emerges from aposematism and scale in poison frogs

Juan C. Santos[a,b,c,1] and David C. Cannatella[a,b]

[a]Section of Integrative Biology and [b]Texas Memorial Museum, University of Texas, Austin, TX 78712; and [c]National Evolutionary Synthesis Center, Durham, NC 27705

Edited by Robert E. Ricklefs, University of Missouri, St. Louis, MO, and approved February 25, 2011 (received for review July 28, 2010)

Complex phenotypes can be modeled as networks of component traits connected by genetic, developmental, or functional interactions. Aposematism, which has evolved multiple times in poison frogs (Dendrobatidae), links a warning signal to a chemical defense against predators. Other traits are involved in this complex phenotype. Most aposematic poison frogs are ant specialists, from which they sequester defensive alkaloids. We found that aposematic species have greater aerobic capacity, also related to diet specialization. To characterize the aposematic trait network more fully, we analyzed phylogenetic correlations among its hypothesized components: conspicuousness, chemical defense, diet specialization, body mass, active and resting metabolic rates, and aerobic scope. Conspicuous coloration was correlated with all components except resting metabolism. Structural equation modeling on the basis of trait correlations recovered "aposematism" as one of two latent variables in an integrated phenotypic network, the other being scaling with body mass and physiology ("scale"). Chemical defense and diet specialization were uniquely tied to aposematism whereas conspicuousness was related to scale. The phylogenetic distribution of the aposematic syndrome suggests two scenarios for its evolution: (*i*) chemical defense and conspicuousness preceded greater aerobic capacity, which supports the increased resource-gathering abilities required of ant–mite diet specialization; and (*ii*) assuming that prey are patchy, diet specialization and greater aerobic capacity evolved in tandem, and both traits subsequently facilitated the evolution of aposematism.

allometry | biodiversity | multivariate | comparative methods

Species display an array of developmentally complex and recurrent phenotypes produced by common ancestry, natural selection, and genetic drift (1, 2). Phenotypic integration is evidenced by developmental, heritable, and functional relationships among different sets of traits that coevolve and give rise to complex phenotypes (1). One such phenotype is aposematism, defined as the co-occurrence of warning signals and defense mechanisms (3). However, other traits (e.g., diet specialization and gregarious behavior) may also contribute to the aposematic phenotype (4). Here, we model the aposematic syndrome in poison frogs as a phenotypic network integrating several traits: conspicuousness, alkaloid sequestration, diet specialization, body mass, and metabolic rates.

A. R. Wallace, who introduced the concept of aposematism, struggled to understand its evolution (5, 6). In aposematism, predators associate conspicuous prey with an unprofitable meal and refrain from attack (7). Thus, defended, the prey may expand its own foraging capabilities (8). The evolution of aposematism is complex for at least four reasons. First, some aposematic organisms synthesize or sequester defensive compounds (9). Second, conspicuousness (high contrast relative to background) signals to the predator that an attack is costly (10). Third, conspicuousness and defense originate in tandem or coevolve (11, 12). Finally, aposematism is at times associated with other traits (e.g., diet specialization) (3).

The term scale is used to reflect the high correlation between body mass (size) and metabolism; it includes aspects of maintenance, growth, and reproduction (13). Effectiveness of defensive signals is related to organismal size (scale) (14), which has allometric consequences for physiological processes (15). Therefore, metabolic rates may be related to the origin and maintenance of aposematism.

Two metabolic parameters commonly studied in ectotherms are resting and active metabolic rates (i.e., RMR and AMR). RMR is the minimal energetic cost to sustain life during inactivity, in controlled temperature, and in a postabsorptive status (16). In contrast, AMR is the upper energetic cost of physical activity by locomotor muscles at their aerobic maximum (17, 18). The difference between AMR and RMR is aerobic scope (hereafter, scope), which generally reflects physical activity and athletic prowess (16). However, most comparative studies use only RMRs (19).

Likewise, phenotypic integration, which we model as a network of dependent relationships among organismal traits, is rarely explored using phylogenetic methods (1). Poison frogs (Dendrobatidae) are perhaps unparalleled for this purpose because a well-supported phylogeny exists (20) and because preliminary data suggest that diverse traits related to aposematism are correlated (12, 21). For example, aposematism and diet specialization (e.g., on ants and mites) repeatedly coevolved in this clade of >290 diurnal species; thus inconspicuous/diet-generalist and aposematic/diet-specialist species are at times close relatives (12). Poison frogs obtain chemical defenses (mostly lipophilic alkaloids; *SI Text* and Fig. S1) from certain arthropod prey: indeed, frogs reared only on nontoxic prey are not chemically defended (22). Alkaloid-defended species thus tend to be diet specialists. In addition to unpalatability from alkaloid defense, conspicuousness of the frogs is relevant because the aposematic signal appears to be directed to close-range predators, mostly snakes and spiders (*SI Text*). Aposematism is also correlated with larger organism size, which in turn is related to metabolic rates (13). An association between metabolic rates and aposematism was suggested for poison frogs (23, 24), but physiological data were limited to seven species, and phylogenetic effects were not considered.

We had five objectives: first, to analyze RMR and AMR across Anura and compare these results with new metabolic data for 54 species of poison frogs; second, to estimate phylogeny and reconstruct ancestral states of component traits in the same species; third, to characterize phenotypic integration with a multivariate model of aposematism using phylogeny-based path analysis (25) and structural equation modeling (SEM) (26); fourth, to test this model against alternative models; and finally, we discuss phenotypic integration and propose two scenarios for the evolution of aposematism in dendrobatids.

Author contributions: J.C.S. and D.C.C. designed research; J.C.S. performed research; J.C.S. contributed new reagents/analytic tools; J.C.S. analyzed data; and J.C.S. and D.C.C. wrote the paper.

The authors declare no conflict of interest.

This article is a PNAS Direct Submission.

Data deposition: The sequences reported in this paper have been deposited in the GenBank database. Accession numbers are in Tables S3 and S4.

[1]To whom correspondence should be addressed. E-mail: juan.santos@duke.edu.

This article contains supporting information online at www.pnas.org/lookup/suppl/doi:10.1073/pnas.1010952108/-/DCSupplemental.

Results and Discussion

Metabolic Characterization of Anurans and Poison Frogs. The analysis of Anura included published data on AMR and RMR from 87 species (Fig. 1, Fig. S2, and Tables S1, S2, and S3). Our regressions of RMR and AMR vs. body mass agreed with published allometric coefficients for *a* (i.e., unit-mass oxygen consumption in mL $O_2 \cdot h^{-1} \cdot g^{-1}$) and exponents for *b* (slope of oxygen consumption). Similar values were found using regressions with phylogenetically independent contrasts (PIC). We found that *a* showed an increase in oxygen consumption from 20 to 25 °C as indicated by the Q_{10} of 2.77 (RMR) and 4.25 (AMR). Additionally, our estimates of *b* for RMR were ∼0.75, similar to the 3/4 allometric constant (27). In contrast, our estimates of *b* for AMR were ∼1.0, indicating isometry as in endotherms (18). Thus, for frogs in general, temperature increases the allometric coefficient *a* (16), RMR scales as predicted for fractal oxygen transport (13, 27), and AMR scales isometrically as expected from targeted oxygen supply to skeletal muscles (17).

On the basis of our data from 54 poison frog species (Table S4), estimated allometric coefficients were similar to those of Anura (Fig. 1*C* and Table S1). At 25 ± 0.5 °C, *a* was 0.169 for RMR and 1.148 for AMR. This result suggests a 5.7- to 6.8-fold increase in oxygen consumed per gram from resting (RMR) to nonsustainable exercise (AMR). In contrast, *b* for all rates was ∼0.781 under ordinary least squares (OLS). However, *b* from PIC regression was ∼0.863, but after removing outlier contrasts (Fig. 1*C*), the exponents were similar to the OLS estimates. For poison frogs, RMR and AMR differ in allometric coefficients *a*, whereas *b* for both RMR and AMR is ∼0.75. Therefore, poison frogs have a nearly constant rate of oxygen consumption per unit mass, regardless of the level of physical activity.

At least three hypotheses might explain the observed differences between Anura and poison frogs. First, poison frog species are small (0.1–10 g) compared with the species of Anura analyzed (0.1–500 g). A similar effect of body size was demonstrated by the analysis of subsamples of the Anura dataset matching the size range of poison frogs (Table S1). Second, the Anura clade encompasses diverse life histories and >250 Myr of evolutionary history (28). In contrast, poison frogs have a more restricted array of life histories (i.e., terrestrial habitats of the Neotropics) and <41 Myr of evolutionary history (20). Third, the Anura data vary in quality (mostly collected before 1985) (16). In contrast, we collected our data under standard conditions.

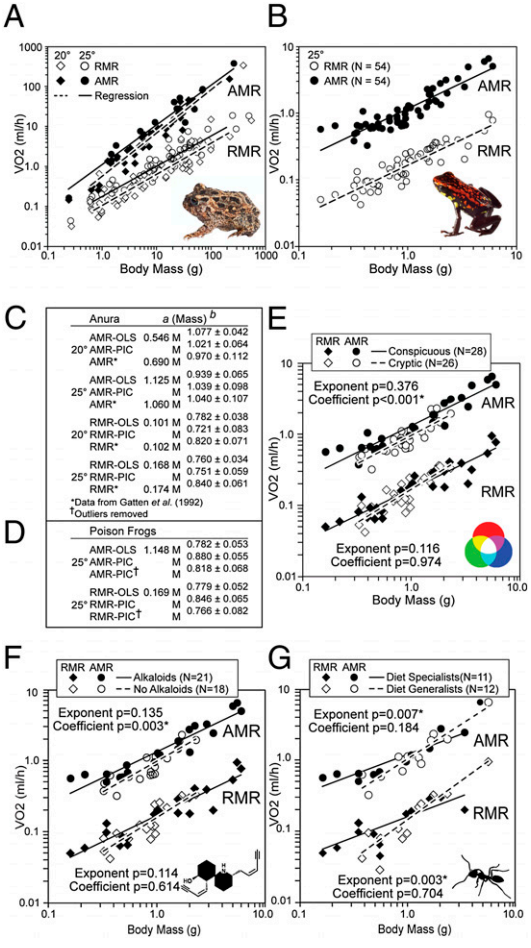

Fig. 1. Active metabolic rate (AMR) and resting metabolic rate (RMR) as functions of body mass and binary states of phenotypes. (*A*) OLS regressions at 20 °C and 25 °C for Anura. (*B*) OLS regressions at 25 ± 0.5 °C for poison frogs. (*C* and *D*) Metabolic rates in mL $O^2 \cdot h^{-1}$ as a function of allometric coefficients *a* in mL $O^2 \cdot h^{-1} \cdot g^{-1}$, mass (grams), and allometric exponent *b* using OLS, phylogenetic independent contrasts (PIC) and PIC without outliers. Published values are AMR* and RMR*. (*E*–*G*) OLS allometric regressions of poison frogs grouped by binary state: (*E*) conspicuousness, (*F*) alkaloid sequestration, and (*G*) diet specialization. *E*–*G* include the probability values of the homogeneity tests for allometric coefficients and exponents (Table S1).

Phylogenetic Analysis of Aposematism, Diet Specialization, Body Mass, and Metabolic Rates. Our phylogenetic analysis detected six origins of conspicuousness, four of alkaloid sequestration, three of diet specialization, and six of large scope (Fig. 2). Two origins of conspicuousness occurred in the absence of alkaloid sequestration: *Allobates zaparo*, a Batesian mimic (29), and *Hyloxalus nexipus*. The remaining four origins of conspicuousness corresponded to aposematism: Clade D, *Hyloxalus azureiventris*, *Epipedobates*, and *Ameerega* clades. Three origins of aposematism were simultaneous with origins of diet specialization: Clade D, *Epipedobates* and *Ameerega* clades; the diet of *H. azureiventris* is unknown. Four origins of large scope co-occurred with all origins of aposematism and Batesian mimicry: *A. zaparo* (mimic), Clade D, *H. azureiventris*, and Clade C (containing *Epipedobates* and *Ameerega*). Therefore, Batesian mimicry and aposematism originated simultaneously or in tandem with greater scope.

Ancestral state reconstructions agreed with the correlation analyses (Table S2). Our results suggest that aposematism, diet specialization, body mass, metabolic rates, and scope covary with the phylogeny (all $\lambda s > 0$). Previous reports (21) of fewer species found that only percentage of ants was independent of phylogeny ($\lambda = 0$). We found a significant phylogenetic effect of ant–mite specialization ($\lambda = 0.605$), suggesting that phylogeny predicts diet specialization. In the pairwise analyses (Table S2), we found significant correlations ($P < 0.01$) between aposematism, diet specialization, body mass, and two measures of aerobic capacity (AMR and scope). These results suggest that the appearance of a phylogenetic correlation between aposematism and aerobic capacity preceded enhanced resource gathering, which in turn promoted diet specialization (8). An alternative explanation is that diet specialization preceded the origin of higher aerobic capacity, assuming prey are a patchy resource (30), with aposematism evolving as a defense against predators. Alkaloid diversity and diet specialization were not associated with body mass or metabolic rates ($P > 0.05$), suggesting that the diversity of alkaloids in prey is highly variable (22).

In the PIC allometric regressions, outlier contrasts (Figs. 1 and 2 and Table S1) are interpreted as grade shifts that support a change in the allometric coefficient *a*, but maintain the exponent *b*, in the context of novel life history traits (31). Five grade shifts are related to large scope in poison frogs: (*i*) three origins of aposematism (*Ameerega* and *Epipedobates* clades and *H. azureiventris*) and (*ii*) five- to sixfold increases in body mass in two aposematic species (*Allobates trivittata* and *Dendrobates sylvaticus*) relative to their sister species. The absence of grade shift for the species-rich aposematic clade (Clade D: *Phyllobates* + *Dendrobates*) is puzzling. Two explanations are plausible: (*i*) species of Clade D are overrepresented and (*ii*) Clade B+C+D

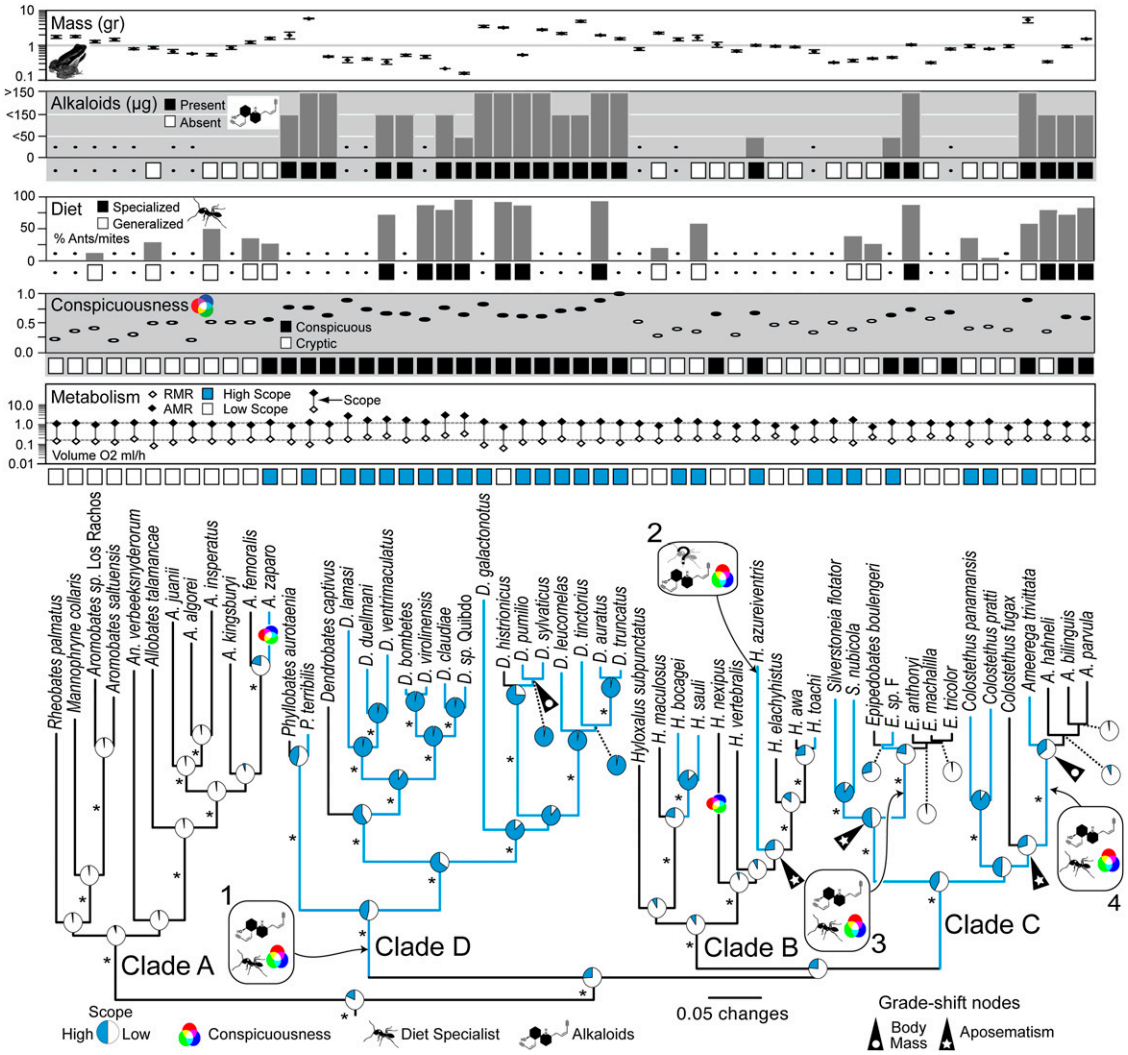

Fig. 2. Poison frog phylogeny, character reconstructions, grade shifts, and variable distributions. Pie charts show the maximum-likelihood reconstructions of scope as the fraction of relative likelihood. The numbered rounded boxes indicate simultaneous origins of conspicuousness (trichrome icon), alkaloid sequestration (alkaloid icon), and diet specialization (ant icon). Grade-shift nodes (increase in allometric coefficient) are presented for aposematism and body mass increases. Bar graphs are the distribution of continuous variables (discrete binned states for alkaloids). Binary state is indicated by solid boxes. Absence (state 0) is indicated by an open box and unknown states by ●. Dashed lines are the mean values for AMR and RMR. Supported nodes (bootstraps = 100% and 1.0 posterior probability = 1.0) are indicated by * in the phylogeny (Fig. S2).

descended from an ancestor with large scope, with subsequent reversals to low aerobic capacity (Fig. 2).

Only one aposeme, *Dendrobates auratus*, has greater aerobic capacity than nonaposematic dendrobatids (23). We expanded on this by incorporating presence/absence dummy variables for conspicuous coloration, alkaloid sequestration, and diet specialization into the metabolic regressions. We then (*i*) compared regressions between binary groups and (*ii*) tested whether inclusion of binary variables significantly increased the fit of the metabolic regressions.

For comparisons between binary groups (Fig. 1 *E*–*G* and Table S1), we found no significant differences ($P > 0.05$) between the allometric exponents (slopes), with the exception of diet. However, the homogeneity of slopes for diet specialization was marginally nonsignificant ($P \sim 0.06$) on the basis of PIC regressions. Therefore, the differences in metabolic rates between the binary groups may be due only to allometric coefficients. Second, we found some significant trends for the metabolic regressions when binary coefficients were included (Table S1). For RMR comparisons, we found no significant ($P > 0.05$) differences between metabolic regressions, and no coefficients from binary analyses were significant. This result suggests that poison frogs do not differ in minimal energetic cost (RMR) regardless of their phenotype. For AMR and scope, we found significant differences ($P < 0.05$) between the binary coefficients on the basis of presence/absence of alkaloid sequestration under both OLS and PIC analyses. This result suggests that in alkaloid-sequestering species, there is a significant increment in the oxygen consumed per gram (OLS increases 40.0% for AMR and 46.9% for scope). However, we also found that conspicuous frogs have a significant ($P < 0.05$) increase in AMR and scope under OLS, but under PIC analyses the effect was nonsignificant ($P > 0.05$). A similar nonsignificant ($P > 0.05$) effect was found for diet specialization. Only the ability to sequester alkaloids is related to increases in aerobic capacity (i.e., AMR and scope).

Multivariate Identification of Integrated Modular Traits. SEM was used to perform a multivariate analysis (Fig. 3 and Fig. S3), which identifies latent variables (32) as complex phenotypes or nodes connecting component traits into phenotypic networks. SEM derives the network structure by reconstructing a variance–covariance (VCV) matrix of the component traits (26). Impor-

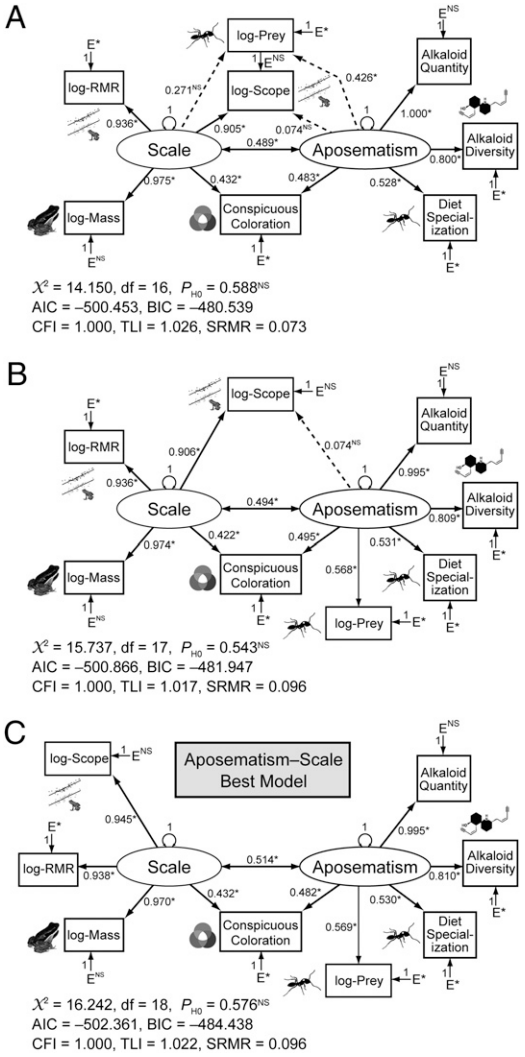

Fig. 3. Phenotypic network models of aposematism and scale integration in poison frogs. (*A*) Scope and mass-dependent diet (log-prey) as a co-dependent with aposematism and scale. (*B*) Scope as a codependent with the aposematism and scale. (*C*) Best model integrating aposematism and scale. Gray ellipses represent latent variables measured by indicator (observable) variables in open boxes. Connecting lines are path coefficients of regressions (single-headed arrows) and correlations (double-headed arrows). Hatched lines are nonsignificant paths. Direct effects are represented by connecting arrows between variables (e.g., scale on log-mass). Indirect effects are compound pathways that connect two variables through an intermediate variable (e.g., scale has an indirect effect on alkaloid quantity via aposematism). Variances of the emergent variables (↺) and regression coefficients of the measurement errors (*E*) were set to 1, which allows a single model to be estimated. Statistics include χ^2 goodness of fit, Akaike information criterion (AIC), Bayesian information criterion (BIC), Bentler's comparative fit index (CFI; >0.95 = good fit), Tucker–Lewis Index (TLI; >0.95 = good fit), and standardized root mean-square residual (SRMR; <0.10 = adequate fit). Model *C* is preferred because it estimates fewer parameters and extra paths (models *A* and *B*) are not significant.

tantly, our VCV matrix needs to be adjusted before the analyses for phylogenetic signal (33, 34). The starting SEM model is proposed on the basis of a priori information such as regression analyses, bivariate correlations, exploratory factor analysis, and theoretical background (32). For an introduction to phylogenetic SEM see *SI Text*.

Our starting model used the following a priori information. First, we used comparative analyses (Table S2) and allometric regressions (Table S1). Second, we performed phylogenetic factor analysis (Table S5). We found two components: (*i*) scale (58.85% of variance) as measured by body mass, scope, and RMR and (*ii*) alkaloid sequestration (19.03% of variance) as measured by alkaloid profiles (quantity and diversity) and ant–mite specialization. However, conspicuous coloration and mean prey number per individual loaded on both components. Third, using background theory and prior knowledge, we identified these latent variables as aposematism and scale (Fig. 3). Specifically, aposematism is the co-occurrence of conspicuousness and defense (11, 12), which also is correlated with diet specialization (21, 24). Scale embodies the correlation between body mass and metabolic rates (35).

Tests of Alternative Models. Our estimated model (Fig. 3*C*) was supported against alternatives: (*i*) six variants with more fixed parameters (Fig. S3) and (*ii*) two variants with locomotor performance (scope) and prey number (log-prey) as codependent on aposematism and scale (Fig. 3 *A* and *B*). We rejected the alternatives because the simpler models (Fig. S3) had significantly worse fit and the more parameterized models (Fig. 3 *A* and *B*) did not fit significantly better than our model. Our best model (Fig. 3*C*) includes three types of variables: indicator, latent, and error. Indicator variables, which are measured directly, include metabolic parameters (scope and RMR), body mass, conspicuousness, diet specialization (prey number and ant–mite specialization), and alkaloid profiles (quantity and diversity). AMR was excluded due to collinearity with scope. Our model recovers two latent variables, interpreted as scale and aposematism. Latent variables are not directly measured and affect the indicators directly; we argue that these represent phenotypic integration of the indicator variables. Scale integrates the indicator variables body mass, metabolic parameters, and conspicuous coloration. Aposematism integrates conspicuous coloration, alkaloid profiles, and diet specialization. Error variables are unexplained variances: measurement error and effects of unaccounted latent variables.

The connecting paths characterize relationships among variables (Fig. 3*C*). Path coefficients are standardized measurements of relationship, and they range from −1 to 1 (i.e., perfect multicollinearity). In our model, significant path coefficients (>0.40) are indicated by *. Nonsignificant path coefficients (∼0) are uninformative and were excluded. Path connectivity represents direct and indirect interactions between variables and a directional representation of the relationship: bivariate correlations (↔), path coefficients (← or →), and fixed variances (↺). A direct path is a relationship between variables that is not explained by other variables. For example, the direct path of aposematism on alkaloid quantity (Fig. 3*C*) is a significant relationship (0.995) not explained by other variables. An indirect path unites direct paths between two variables using intermediates (26).

The interpretation of the indirect paths contrasts with some simpler bivariate correlations (Table S2). For example, scope and alkaloid quantity are highly correlated (Table S2, r_{IC} = 0.515; and Table S5, r_{IC} = 0.519). However, our model suggests a compound relationship: Scope ← scale ↔ aposematism → alkaloid quantity. The interpretation of this compound path is as follows: (*i*) Scope has a direct relationship (path coefficient = 0.945) with scale; (*ii*) scale is correlated (0.514) with aposematism; and (*iii*) aposematism has a direct relationship (0.995) with alkaloid quantity. The strength of this path is the product of its path coefficients (0.945 × 0.514 × 0.995 = 0.483, similar to Table S2: r_{IC} = 0.515). Therefore, the association between alkaloid quantity and scope is a manifestation of the emergent relationship between scale and aposematism. Other compound paths are between the indicators on the same latent variable. For example, alkaloid diversity and ant–mite specialization are positively associated (0.810 × 0.530 = 0.429) as evidenced by their bivariate correlation (Table S2, r_{IC} = 0.466; and Table S5, r_{IC} = 0.466). Thus, alkaloid diversity and ant–mite specialization manifest aposematism. An example of dual indirect–direct paths is evidenced by the relationship of conspicuous coloration and both latents, scale and aposematism. Conspicuous coloration is re-

lated to aposematism by both a direct path (0.482) and an indirect path through scale (i.e., 0.514 × 0.432 = 0.222). The total effect on aposematism is the sum of both paths (i.e., 0.482 + 0.222 = 0.704). The interpretation of the total effect is that conspicuous coloration is a manifestation of both aposematism and scale simultaneously.

Our SEM model has two levels: structural and measurement. The structural portion corresponds to the relationship among latent variables. Specifically, this relationship is represented by codependency or integration between scale and aposematism. The measurement portion is the relationship between indicators and latent variables. For example, scale is related to body mass, metabolic rates, and conspicuousness. The reliability of each indicator on its latent variable is calculated by the square of the path coefficient; values >0.70 are well supported (32). In the measurement portion of our model, scale is measured (predicted) with high reliability by body mass (0.941 = 0.970 × 0.970), scope (0.893), and RMR (0.880). However, scale was measured with low reliability (i.e., weaker prediction) by conspicuous coloration (0.187). Aposematism is measured with high to moderate reliability by alkaloid profiles (quantity, 0.990; diversity, 0.656). However, aposematism was measured with low reliability by conspicuousness (0.232) and diet profiles (ant–mite specialization, 0.281; and prey items, 0.324). Chemical defense (alkaloid quantity and diversity) is the main predictor of aposematism, and conspicuousness and diet specialization are weaker predictors.

Multivariate Characterization of a Complex Phenotype and Alternative Hypotheses. Our SEM model explains aposematism as an example of phenotypic integration (Fig. 3*C*) and it is characterized by these direct paths: (*i*) Changes (e.g., natural selection) on scale are manifested significantly by body mass and metabolic rates; (*ii*) changes on aposematism are manifested strongly by chemical defense (alkaloids), but weakly by diet; and (*iii*) changes on aposematism or scale are manifested by conspicuousness.

The structural portion of the model predicts phenotypic integration between aposematism (such as alkaloid quantity, diet specialization, or conspicuousness) and scale (e.g., scope, RMR, and body mass). Our model predicts that diet specialists maximize their nutritional input (i.e., net energy gain) by ingesting larger numbers of alkaloid-rich prey (e.g., ants), with low nutritional value and expensive processing (30). Several studies (23, 24, 36) support our model interpretation. Specifically, diet-specialized poison frogs are active predators with larger home ranges, will reject other syntopic nutritious prey, but eat large numbers of specialized prey. Therefore, we can predict that diet specialization might revert to a generalist mode if the effectiveness of aposematism is reduced.

Our model also explains the association of greater aerobic capacity (AMR and scope) with aposematism. Two alternative hypotheses characterize the sequence of adaptations leading to the integration of aposematism and scale in poison frogs. First, as a preexisting predator deterrent, aposematism allowed individuals to increase resource-gathering abilities in the form of high aerobic capacity and diet specialization (8). Under this alternative, aposematism initially linked chemical defense with a generalist diet; however, this diet must have included some alkaloid-bearing arthropods. Second, the evolution of diet specialization on alkaloid-bearing arthropods preceded higher aerobic capacity, assuming that prey is a patchy resource (30), and afterward both traits facilitated the acquisition and sequestering of alkaloids and thus the evolution of aposematism as a defense against predators.

We have not considered other variables that might affect the model, such as mate attraction to conspicuous coloration (37), conspicuousness beyond the visible spectrum (e.g., UV perception) (38), and biochemical consequences of alkaloid sequestration (39). Improved metrics of conspicuousness are needed, especially those based on actual spectral reflectance (10) and predator perception in nature (Fig. S4). The evolutionary and ecological dimensions of complex phenotypes are only partly explained by simple bivariate statistical analyses of modular traits. The synthesis of background knowledge, characterization of connectedness among modular traits, and phylogenetic context promises a simultaneous characterization of the factors that contribute to phenotypic diversity.

Materials and Methods

Physiological Parameters and Body Mass. We compiled data on metabolic rates (20 and 25 °C) and body mass (grams) of 87 anuran species (Table S3). All RMRs (VO_2 mL·h^{-1} after resting) were analyzed (16). We analyzed only AMRs (VO_2 mL·h^{-1} after nonsustainable exercise) from manual and motor rotation experiments (16). Both AMR methods were comparable (*SI Text*). The effect of temperature on metabolic parameters was determined using $Q_{10} = (R_2/R_1)^{10/(T_2 - T_1)}$, where R_1 and R_2 are metabolic parameters at temperatures T_1 and T_2 (°C) such that $T_1 < T_2$ (19). We collected data at 24.5–25.5 °C from 474 individuals of 54 species of poison frogs (Table S4). The data included AMR (measured following nonsustainable exercise by manual rotation), RMR, and aerobic scope (scope = AMR − RMR). Body weight was recorded to 0.01 g, and all physiological measurements were repeated two to three times per individual. Animal handling followed Institutional Animal Care and Use Committe guidelines (05111001) (*SI Text*). Binary classification of metabolic rates was 0 (low), if the species has a negative residual for the metabolic parameter regressed on body mass, and otherwise 1 (high).

Conspicuous Coloration, Alkaloid, and Diet Profiles. We estimated conspicuous coloration (Table S4) using a "pixel count" approach (11). Our technique is summarized from *SI Text*: (*i*) Photographs of frogs under standardized conditions were divided into background (leaf litter) and frog body areas; (*ii*) each body area was sampled for polygons of homogeneous color, the pixels in each polygon were counted, and the means of luminosity and primary color channels [red, green, and blue (RGB)] were calculated; (*iii*) MANCOVA (luminosity as a covariate) was used to predict each RGB value under constant brightness for each polygon; (*iv*) cluster analysis for the leaf litter RGB data identified a background centroid; (*v*) the measurement of raw conspicuousness of each polygon was determined as its Euclidean distance to the centroid; (*vi*) a weighted measure of conspicuousness was calculated; and (*vii*) all weighted distances were summed as a species score. Conspicuousness was 0 (cryptic) if the score was ≤57.69 (the mean of all species) and 1 (conspicuous) if it was >57.69.

We compiled skin alkaloid profiles from published accounts of 34 dendrobatid species, and we collected data from 6 species using TLC (Fig. S1 and Table S4) (21). Species alkaloid profiles were characterized by presence, quantity, and diversity of alkaloids. Presence is 1, if ability to sequester alkaloids was detected; and inability is 0. Quantity is the abundance in 100 mg of skin: state 0 (no alkaloids), 1 (<50 μg), 2 (>50 and <150 μg), and 3 (>150 μg). Diversity is the number of classes reported per species (40).

Diet was characterized using three variables (Table S4). Ant–mite specialization is the percentage of ants and mites in the diet. Mean number of prey per individual is a mass-dependent measure calculated from gut content data (21, 36). Niche breadth is the inverse of Simpson's index (21): $B = 1/(\sum_{i=1}^{n} p_i^2)$, where i is prey category, p is proportion of resource category, and n is total of categories. Diet specialization was 0 (generalist) if the species has a diet of ≤70% of ants and mites and niche breadth >0.15 and 1 (specialist) if otherwise.

Phylogenetic Estimation. We inferred a phylogeny of Anura from 121 species (Fig. S2 and Table S3). The molecular data for Anura included only mitochondrial genes (mtDNA: ~2,400 bp). The phylogeny of poison frogs was inferred from the 54 species for which physiological data were collected (Table S4). We used eight mitochondrial genes (~4.5 kb) and seven nuclear genes (~5.0 kb). GenBank numbers and PCR conditions are in Table S4 and *SI Text*. Protocols of DNA sequencing and alignment are described in refs. 12, 20, and 41. Both datasets were analyzed with maximum-likelihood (ML) and Bayesian phylogenetics (*SI Text*). Node support was assessed by 500 bootstraps (ML) and posterior probabilities (Bayesian). All tree topologies agreed, so the best ML trees were used.

Statistical Methods. For comparative methods, continuous variables were normalized (33, 34). We used least-squares regressions (OLS) and PIC regressions of metabolic rates vs. body mass for both Anura and poison frogs. The OLS model (16) was $\log(y) = a + (b \times x)$, where y is AMR or RMR, a is the allometric coefficient, b is the allometric exponent, and x is log (mass). A subset of species from the Anura physiology dataset matching the poison frog size range (0.1–10 g) was used to compare our estimates of metabolic parameters, using bootstrap and jackknife approaches. In a com-

plementary analysis for poison frogs, we included binary (dummy) variables for conspicuousness, alkaloid sequestration, or diet specialization in the model: $\log(y) = a + (b_{binary} \times z) + (b \times x)$, where y is AMR, RMR, or scope; a is the allometric coefficient; b_{binary} is the coefficient of binary variable; z is the binary variable; b is the allometric exponent; and x is log (mass). For PIC regressions, we used the ML phylogenies with log-transformed standardized branch lengths (34) and we calculated PICs using PDAP:PTREE (42) in Mesquite (43). PIC regressions were fit through the origin and regression coefficients were tested at $\alpha = 0.05$ (34). We detected outlier contrasts (grade shifts) in allometric regressions by comparing the regressions and excluding outlier residuals (31).

Ancestral states were estimated using the mk1 model in Mesquite (43); the probability of a state was reported as raw likelihood. We validated our reconstructions by estimating the mean posterior probability of each character state per node from 5,000 samples using BayesTraits (44). Because the results from both methods were similar, only those of Mesquite are reported. Pairwise correlations between traits were estimated using phylogenetic generalized least squares (44) and PIC. We analyzed the covariance of each trait and the phylogeny using λ in BayesTraits (44) and tested each λ against the hypothesis of phylogenetic independence (H_0: $\lambda = 0$). We then calculated the phylogenetic pairwise correlation coefficients by including λ as a free parameter. Significance was determined against independence (H_0: $r = 0$). These results were validated using PIC regressions in Mesquite.

Phylogenetic SEM. We used a multivariate phylogenetic method based on path analysis (25) and SEM (26). The species sample ($n = 21$, Table S4) has measurements for all variables. Our technique is summarized as follows: (*i*) multivariate normality was tested; (*ii*) the phylogeny-enhanced variance–covariance matrix (**S**) was estimated using the bivariate correlation matrix **R** (Table S5) and the SDs of the PICs were calculated using matrix algebra; (*iii*) phylogenetic principal component analysis (PPCA) and principal axis factoring (PPFA) with varimax orthogonal rotation (Table S5) were used to propose an initial SEM model; (*iv*) this model was fit to the **S** matrix in MPlus (45); (*v*) fit statistics included χ^2 goodness of fit and complementary fit indexes; (*vi*) SEM models were compared using their fit indexes and estimated parameters; and (*vii*) the interpretation of the best model was based on a priori information and network structure. For an extended introduction see *SI Text*.

ACKNOWLEDGMENTS. J.C.S. thanks A. Woods, C. Barrio-Amorós, A. Amézquita, C. O. Wilke, the D.C.C. laboratory, the Smithsonian Tropical Research Institute, and L. A. Coloma. In particular, J.C.S. and D.C.C. acknowledge one anonymous reviewer for perceptive comments. J.C.S. thanks N. Biani and I. Santos for their kindness and support. J.C.S. and D.C.C. acknowledge collection permits from Panamá, Ecuador, and Venezuela. D.C.C. was supported by National Science Foundation Grant EF-0334952. J.C.S. was supported by University of Texas fellowships and National Science Foundation Doctoral Dissertation Improvement Grant DEB-0710033 and National Evolutionary Synthesis Center Grants EF-0423641 and EF-0905606.

1. Pigliucci M, Preston K (2004) *Phenotypic Integration: Studying the Ecology and Evolution of Complex Phenotypes* (Oxford Univ Press, New York).
2. West-Eberhard MJ (2003) *Developmental Plasticity and Evolution* (Oxford Univ Press, New York).
3. Ruxton GD, Sherratt TN, Speed MP (2004) *Avoiding Attack: The Evolutionary Ecology of Crypsis, Warning Signals & Mimicry* (Oxford Univ Press, Oxford).
4. Tullberg BS, Hunter AF (1996) Evolution of larval gregariousness in relation to repellent defenses and warning coloration in tree-feeding Macrolepidoptera: A phylogenetic analysis based on independent contrasts. *Biol J Linn Soc Lond* 57: 253–276.
5. Wallace AR (1867) Mimicry and other protective resemblances among animals. *Westminster Foreign Q Rev* 32:1–43.
6. Speed MP, Ruxton GD (2005) Aposematism: What should our starting point be? *Proc Biol Sci* 272:431–438.
7. Alatalo RV, Mappes J (1996) Tracking the evolution of warning signals. *Nature* 382: 708–710.
8. Speed MP, Brockhurst MA, Ruxton GD (2010) The dual benefits of aposematism: Predator avoidance and enhanced resource collection. *Evolution* 64:1622–1633.
9. Broom M, Speed MP, Ruxton GD (2005) Evolutionarily stable investment in secondary defences. *Funct Ecol* 19:836–843.
10. Endler JA (1990) On the measurement and classification of color in studies of animal color patterns. *Biol J Linn Soc Lond* 41:315–352.
11. Summers K, Clough ME (2001) The evolution of coloration and toxicity in the poison frog family (Dendrobatidae). *Proc Natl Acad Sci USA* 98:6227–6232.
12. Santos JC, Coloma LA, Cannatella DC (2003) Multiple, recurring origins of aposematism and diet specialization in poison frogs. *Proc Natl Acad Sci USA* 100: 12792–12797.
13. West GB, Brown JH, Enquist BJ (1999) The fourth dimension of life: Fractal geometry and allometric scaling of organisms. *Science* 284:1677–1679.
14. Forsman A, Herrstrom J (2003) Asymmetry in size, shape, and color impairs the protective value of conspicuous color patterns. *Behav Ecol* 15:141–147.
15. Evans DL, Schmidt JO, eds (1990) *Insect Defenses: Adaptive Mechanisms and Strategies of Prey and Predators* (State University of New York Press, New York).
16. Gatten RE, Miller KJ, Full RJ (1992) Energetics at rest and during locomotion. *Environmental Physiology of the Amphibians*, eds Feder ME, Burggren WW (Univ of Chicago Press, Chicago).
17. Weibel ER, Bacigalupe LD, Schmitt B, Hoppeler H (2004) Allometric scaling of maximal metabolic rate in mammals: Muscle aerobic capacity as determinant factor. *Respir Physiol Neurobiol* 140:115–132.
18. Bishop CM (1999) The maximum oxygen consumption and aerobic scope of birds and mammals: Getting to the heart of the matter. *Proc Biol Sci* 266:2275–2281.
19. Hillman SS, Withers PC, Drewes RC, Hillyard SD (2009) *Ecological and Environmental Physiology of Amphibians* (Oxford Univ Press, Oxford).
20. Santos JC, et al. (2009) Amazonian amphibian diversity is primarily derived from late Miocene Andean lineages. *PLoS Biol* 7:e56.
21. Darst CR, Menéndez-Guerrero PA, Coloma LA, Cannatella DC (2005) Evolution of dietary specialization and chemical defense in poison frogs (Dendrobatidae): A comparative analysis. *Am Nat* 165:56–69.
22. Saporito RA, Spande TF, Garraffo HM, Donnelly MA (2009) Arthropod alkaloids in poison frogs: A review of the 'dietary hypothesis'. *Heterocycles* 79:277–297.
23. Pough FH, Taigen T (1990) Metabolic correlates of the foraging and social-behavior of dart-poison frogs. *Anim Behav* 39:145–155.
24. Toft CA (1981) Feeding ecology of Panamanian litter anurans: Patterns of diet and foraging mode. *J Herpetol* 15:139–144.
25. Wright S (1984) Diverse uses of path analysis. *Human Population Genetics*, ed Chakravarti A (Van Nostrand Reinhold, New York), pp 1–34.
26. Grace JB (2006) *Structural Equation Modeling and Natural Systems* (Cambridge Univ Press, Cambridge, UK).
27. West GB, Brown JH, Enquist BJ (1997) A general model for the origin of allometric scaling laws in biology. *Science* 276:122–126.
28. Wells KD (2007) *The Ecology and Behavior of Amphibians* (Univ of Chicago Press, Chicago).
29. Darst CR, Cummings ME (2006) Predator learning favours mimicry of a less-toxic model in poison frogs. *Nature* 440:208–211.
30. Huey RB, Pianka ER (1981) Ecological consequences of foraging mode. *Ecology* 62: 991–999.
31. Nunn CL, Barton RA (2000) Allometric slopes and independent contrasts: A comparative test of Kleiber's law in primate ranging patterns. *Am Nat* 156:519–533.
32. Kline R (2005) *Pinciples and Practice of Structural Equation Modeling* (Guilford Press, New York).
33. Felsenstein J (1985) Phylogenies and the comparative method. *Am Nat* 125:1–15.
34. Garland T, Harvey PH, Ives AR (1992) Procedures for the analysis of comparative data using phylogenetically independent contrasts. *Syst Biol* 41:18–32.
35. Schmidt-Nielsen K (1984) *Scaling: Why Is Animal Size So Important?* (Cambridge Univ Press, Cambridge, UK).
36. Caldwell JP (1996) The evolution of myrmecophagy and its correlates in poison frogs (family Dendrobatidae). *J Zool (Lond)* 240:75–101.
37. Summers K, Symula R, Clough M, Cronin T (1999) Visual mate choice in poison frogs. *Proc Biol Sci* 266:2141–2145.
38. Honkavaara J, Koivula M, Korpimaki E, Siitari H, Viitala J (2002) Ultraviolet vision and foraging in terrestrial vertebrates. *Oikos* 98:505–511.
39. Daly JW, et al. (2003) Evidence for an enantioselective pumiliotoxin 7-hydroxylase in dendrobatid poison frogs of the genus Dendrobates. *Proc Natl Acad Sci USA* 100: 11092–11097.
40. Daly JW, Garraffo HM, Spande TF (1999) Alkaloids from amphibian skins. *Alkaloids: Chemical and Biological Perspectives*, ed Pelletier SW (Pergamon, New York), pp 1–161.
41. Darst CR, Cannatella DC (2004) Novel relationships among hyloid frogs inferred from 12S and 16S mitochondrial DNA sequences. *Mol Phylogenet Evol* 31:462–475.
42. Midford PE, Garland T, Maddison WP (2005) *PDAP Package of Mesquite*, ver 1.14. Available at http://mesquiteproject.org/pdap_mesquite/. Accessed December 15, 2009.
43. Maddison WP, Maddison DR (2009) *Mesquite: A Modular System for Evolutionary Analysis*, ver 2.72. Available at http://mesquiteproject.org. Accessed December 15, 2009.
44. Pagel M, Meade A (2007) *BayesTraits* (Univ of Reading, Reading, UK), ver 1.0. Available at http://www.evolution.rdg.ac.uk/BayesTraits.html. Accessed December 15, 2009.
45. Muthén BO, Muthén LK (2008) *Mplus,* Los Angeles, ver 5. Available at http://statmodel.com. Accessed December 20, 2009.